J. Fluid Mech. (2010), *vol.* 664, *pp.* 297–312.
doi:10.1017/S0022112010003824

Prandtl–Blasius temperature and velocity boundary-layer profiles in turbulent Rayleigh–Bénard convection

QUAN ZHOU[1], RICHARD J. A. M. STEVENS[2], KAZUYASU SUGIYAMA[2,3], SIEGFRIED GROSSMANN[4], DETLEF LOHSE[2] AND KE-QING XIA[5]†

[1]Shanghai Institute of Applied Mathematics and Mechanics, Shanghai University, Shanghai 200072, China

[2]Physics of Fluids Group, Department of Science and Technology, J. M. Burgers Centre for Fluid Dynamics, and Impact-Institute, University of Twente, 7500 AE Enschede, The Netherlands

[3]Department of Mechanical Engineering, School of Engineering, The University of Tokyo, 7-3-1 Hongo, Bukyo-ku, Tokyo 113-8756, Japan

[4]Fachbereich Physik, Philipps-Universität Marburg, D-35032 Marburg, Germany

[5]Department of Physics, The Chinese University of Hong Kong, Shatin, Hong Kong, China

(Received 5 February 2010; revised 12 July 2010; accepted 12 July 2010; first published online 8 September 2010)

The shapes of the velocity and temperature profiles near the horizontal conducting plates' centre regions in turbulent Rayleigh–Bénard convection are studied numerically and experimentally over the Rayleigh number range $10^8 \lesssim Ra \lesssim 3 \times 10^{11}$ and the Prandtl number range $0.7 \lesssim Pr \lesssim 5.4$. The results show that both the temperature and velocity profiles agree well with the classical Prandtl–Blasius (PB) laminar boundary-layer profiles, if they are re-sampled in the respective dynamical reference frames that fluctuate with the instantaneous thermal and velocity boundary-layer thicknesses. The study further shows that the PB boundary layer in turbulent thermal convection not only holds in a time-averaged sense, but is most of the time also valid in an instantaneous sense.

Key words: Bénard convection, boundary layers, convection

1. Introduction

The turbulent motion in a fluid layer sandwiched by two parallel plates and heated from below and cooled from above, i.e. Rayleigh–Bénard (RB) convection, has become a fruitful paradigm for understanding the physical nature of a wide range of complicated convection problems occurring in nature and in engineering (Siggia 1994; Ahlers, Grossmann & Lohse 2009; Lohse & Xia 2010). A key issue in the study of turbulent RB systems is to understand how heat is transported upwards by turbulent flow across the fluid layer. It is measured in terms of the Nusselt number Nu, defined as $Nu = J/(\chi \Delta/H)$, which depends on the turbulent intensity and the fluid properties. These are characterized, respectively, by the Rayleigh number Ra and the Prandtl number Pr, namely $Ra = \alpha g H^3 \Delta/\nu\kappa$ and $Pr = \nu/\kappa$. Here, J is the heat

† Email address for correspondence: kxia@phy.cuhk.edu.hk

current density across the fluid layer with height H and with an applied temperature difference Δ, χg is the gravitational acceleration, and α, ν and κ are, respectively, the thermal expansion coefficient, kinematic viscosity and thermal diffusivity of the convecting fluid, for which the Oberbeck–Boussinesq approximation is considered as valid. As heat transport is controlled by viscous and thermal diffusions in the immediate vicinity of the solid boundaries, Nu is intimately related to the physics of the boundary layers (BLs).

In thermal convective turbulent flow, two types of BLs exist near the top and bottom plates, both of which are generated and stabilized by the viscous shear of the large-scale mean flow: one is the kinematic BL and the other is the thermal BL. The two layers are not isolated, but are coupled dynamically to each other. Both layers play an essential role in turbulent thermal convection, especially for the global heat flux across the fluid layer. The relation between the shear rate and the heat flux depends crucially on the shape of the temperature profile (see, e.g. Ching 1997). Furthermore, almost all theories proposed to predict the relation between Nu and the control parameters Ra and Pr are based on some kind of assumptions for the BLs, such as the stability assumption of the thermal BL from the early marginal stability theory (Malkus 1954), the turbulent-BL assumption from the theories of Shraiman & Siggia (1990) and Siggia (1994) and of Dubrulle (2001, 2002) and the Prandtl–Blasius (PB) laminar-BL assumption of the Grossmann & Lohse (GL) theory (Grossmann & Lohse 2000, 2001, 2002, 2004). Because of the complicated nature of the problem, different theories based on different assumptions for the BL may yield the same predictions for the global quantities, such as the Nu–Ra scaling relation (Castaing *et al.* 1989; Shraiman & Siggia 1990). Therefore, direct characterization of the BL properties is essential for the differences between and the testing of the various theoretical models, and will also provide insight into the physical nature of turbulent heat transfer in the RB system.

In the GL theory, the kinetic energy and thermal dissipation rates have been decomposed into BL and bulk contributions. Scaling-wise and in a time-averaged sense, a laminar Prandtl–Blasius BL has been assumed. This theory can successfully describe and predict the Nusselt and the Reynolds number dependences on Ra and Pr (see, e.g. the recent review in Alhers *et al.* 2009). As the PB laminar BL is a key ingredient of the GL theory, it is important to make direct experimental verification of it. We also note that the (experimentally verified) calculation of the mean temperature in the bulk in both liquid and gaseous non-Oberbeck–Boussinesq RB flows (Ahlers *et al.* 2006, 2007, 2008) is based on the PB theory.

In a recent high-resolution measurement of the properties of the velocity BL, Sun, Cheung & Xia (2008) have found that, despite the intermittent emission of plumes, the PB-type laminar BL description is indeed a good approximation, in a time-averaged sense, both in terms of its scaling and its various dynamical properties. However, because of the intermittent emissions of thermal plumes from the BLs, the detailed dynamics of both kinematic and thermal BLs in turbulent RB flow are much more complicated. On the one hand, direct comparisons of experimental velocity (du Puits, Resagk & Thess 2007) and numerical temperature (Shishkina & Thess 2009) profiles with theoretical predictions have shown that both the classical PB laminar BL profile and the empirical turbulent logarithmic profile are not good approximations for the time-averaged velocity and temperature profiles. Furthermore, Sugiyama *et al.* (2009) from two-dimensional (2D) and Stevens, Verzicco & Lohse (2010) from three-dimensional (3D) numerical simulations found that the deviation of the BL profile from the PB profile increases from the plate's centre towards the sidewalls, due to the

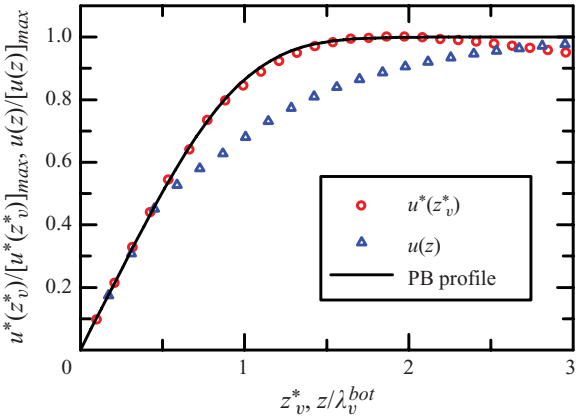

FIGURE 1. (Colour online) Comparison between the spatial x-interval and time-averaged velocity profiles $u(z)$ (triangles), the dynamically re-scaled velocity profile $u^*(z_v^*)$ (circles – for the notation we refer to § 3) and the PB velocity profile (solid line) near the bottom plate obtained experimentally at $Ra = 1.8 \times 10^{11}$ and $Pr = 5.4$ (working fluid water).

rising (falling) plumes near the sidewalls. On the other hand, Qiu & Xia (1998) have found near the sidewall and Sun *et al.* (2008) near the bottom plate that the velocity BL obeys the scaling law of the PB laminar BL, i.e. its width scales as $\lambda_v/H \sim Re^{-0.5}$, where λ_v is the kinematic BL thickness, defined as the distance from the wall at which the extrapolation of the linear part of the local mean horizontal velocity profile $u(z) = \langle u_x(z,t)\rangle$, with z being the vertical distance from the bottom plate and $\langle\cdots\rangle$ being the time average at the plate centre, meets the horizontal line passing through the maximum horizontal velocity $[u(z)]_{max}$ and $Re = [u(z)]_{max} H/\nu$ is the Reynolds number based on $[u(z)]_{max}$. These papers highlight the need to study the nature of the BL profiles, both velocity and temperature, in turbulent thermal RB convection.

Considerable progress on this issue has recently been achieved by Zhou & Xia (2010) who have experimentally studied the velocity BL for water ($Pr = 4.3$) with particle image velocimetry (PIV). They found that, since the dynamics above and below the range of the BL is different, a time average at a fixed height, z, above the plate with respect to the laboratory (or container) frame will sample a mixed dynamics, one pertaining to the BL range and the other one pertaining to the bulk, because the measurement position will be sometimes inside and sometimes outside the fluctuating width of the BL. To make a clean separation between the two types of dynamics, Zhou & Xia (2010) studied the BL quantities in a time-dependent frame that fluctuates with the instantaneous BL thickness itself. Within this dynamical frame, they found that the mean velocity profile agrees well with the theoretical PB laminar BL profile. In figure 1, we show the essence of the results, again for the velocity BL but for somewhat larger Pr, now $Pr = 5.4$. (For details of the experiment and the apparatus used, see Xia, Sun & Zhou 2003; Zhou & Xia 2010.) It is seen here that the method of using the time dependent frame works equally well as for the $Pr = 4.3$ case of Zhou & Xia (2010). While at the large $Ra = 1.8 \times 10^{11}$ the time- and space-averaged velocity profile (triangles) already deviates considerably from the PB profile (solid line), the dynamically re-scaled profile (circles) perfectly agrees with the PB profile. Thus a dynamical algorithm has been established to directly characterize the BL properties in turbulent RB systems, which is mathematically well-defined and requires no adjustable parameters.

The questions which immediately arise are as follows: (i) Does this dynamical re-scaling method also work for the temperature field, giving good agreement with the (Prandtl number dependent) PB temperature profile? (ii) And does the method also work for lower Pr, where the velocity field is more turbulent? Both these questions cannot be answered with the current Hong Kong experiments, as PIV only provides the velocity field and not the temperature field, and as PIV has not yet been established in gaseous RB flows, i.e. in low Pr RB flows.

In this paper, we will answer these two questions with the help of direct numerical simulations (DNS). To avoid the complications of oscillations and rotations of the large-scale convection roll plane and as the PB theory is a 2D theory anyhow we will restrict ourselves to the 2D simulations of Sugiyama *et al.* (2009). Our results will show that Zhou & Xia's (2010) idea of using time-dependent coordinates to disentangle the mixed dynamics of BL and bulk works excellently also for the temperature field and for low Pr flow. That is, if dynamically re-scaled, both velocity and temperature BL profiles can be brought into excellent agreement with the theoretical Prandtl–Blasius BL predictions, for both larger and lower Pr.

2. DNS of the two-dimensional Oberbeck–Boussinesq equations

The numerical method has been explained in detail in Sugiyama *et al.* (2009). In a nutshell, the Oberbeck–Boussinesq equations with no-slip velocity boundary conditions at all four walls are solved for a 2D RB cell with a fourth-order finite-difference scheme. The aspect ratio is $\Gamma \equiv D/H = 1.0$. Four sets of data are presented here, their Rayleigh number, Ra, Prandtl number, Pr and the corresponding Reynolds number, Re, are (10^8, 0.7, 5.4×10^3); (10^9, 0.7, 1.9×10^4); (10^8, 4.3, 8.3×10^2) and (10^9, 4.3, 3.2×10^3), respectively. In all the computations, the kinematic viscosity, thermal expansion coefficient and the temperature difference were fixed at $\nu = 6.6945 \times 10^{-7}$ m^2 s^{-1}, $\alpha = 3.8343 \times 10^{-4}$ K^{-1} and $\Delta = 40$ K, respectively. The cell height was $H = 7.524$ cm for $Ra = 10^8$ and $Pr = 0.7$, $H = 4.108$ cm for $Ra = 10^8$ and $Pr = 4.3$, $H = 16.21$ cm for $Ra = 10^9$ and $Pr = 0.7$ and $H = 8.851$ cm for $Ra = 10^9$ and $Pr = 4.3$. Sugiyama *et al.* (2009) have provided a detailed code validation.

As the governing equations are strictly Oberbeck–Boussinesq, there exists a top–bottom symmetry. We therefore discuss only the velocity and temperature profiles near the bottom plate. For the temperature profiles, we introduce the non-dimensional temperature $\Theta(z, t)$, defined as

$$\Theta(z, t) = \frac{\theta^{bot} - \theta(z, t)}{\Delta/2}, \tag{2.1}$$

where θ^{bot} is the temperature of the bottom plate. In this definition, $\Theta(H) = 2$ and $\Theta(0) = 0$ are the temperatures of the top and bottom plates, respectively, and $\Theta(H/2) = 1$ is the mean bulk temperature.

3. Dynamical boundary-layer rescaling

The idea of the Zhou & Xia (2010) method is to construct a dynamical frame that fluctuates with the local instantaneous BL thickness. To do this, first the instantaneous kinematic and thermal BL thicknesses are determined using the algorithm introduced by Zhou & Xia (2010). To reduce data scatter, the horizontal velocity and temperature profiles at each discrete time t, $u(z, t)$ and $\Theta(z, t)$, are obtained by averaging the velocity and temperature fields along the x-direction (horizontal) over the range

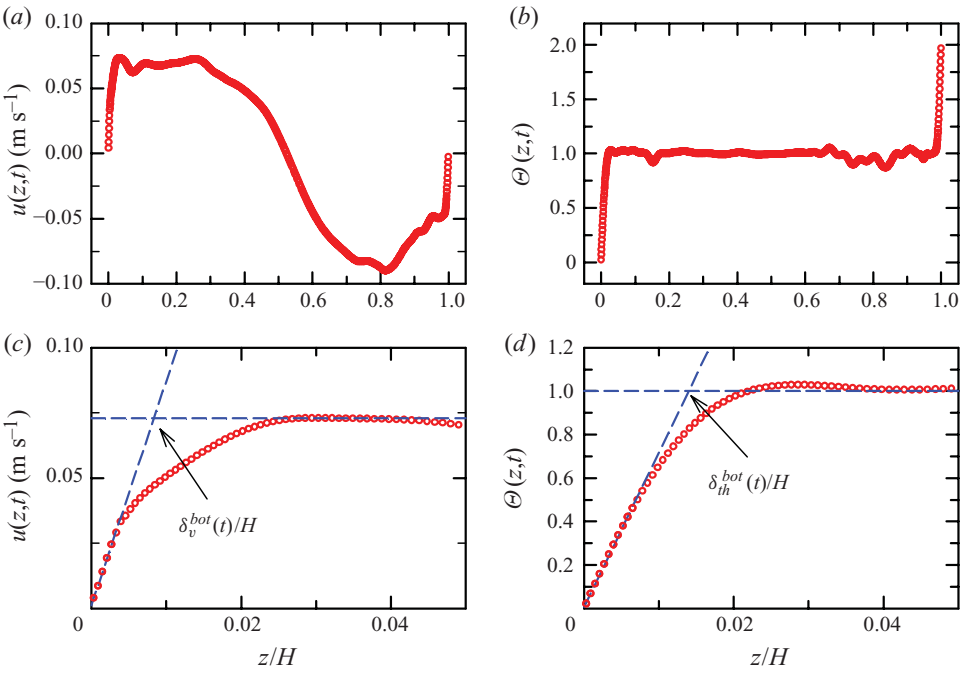

FIGURE 2. (Colour online) Examples of (*a*) an instantaneous horizontal velocity profile $u(z,t)$ and (*b*) a normalized instantaneous temperature profile $\Theta(z,t)$, averaged over $0.475 < x/D < 0.525$. The DNS data are obtained at $Ra = 10^9$ and $Pr = 0.7$. (*c*) and (*d*) Enlarged portions of the velocity and temperature profiles near the bottom plate, respectively. The two tilted dashed lines are linear fits to the linear parts of the velocity and temperature profiles near the plate and the two horizontal dashed lines mark the instantaneous maximum horizontal velocity and the bulk temperature $\Theta = 1$, respectively. The distances of the crossing points from the plate define the instantaneous BL thicknesses $\delta_{v,th}^{bot}(t)$. The instantaneous profiles are not top-down symmetric, while the time averaged ones are top-down symmetric. Within the present statistical error, our data are consistent with zero thermal gradient in the bulk.

$0.475 < x/D < 0.525$. Figures 2(*a*) and 2(*b*) show examples of $u(z,t)$ and $\Theta(z,t)$ versus the normalized height z/H, respectively, of the DNS data obtained at $Ra = 10^9$ and $Pr = 0.7$. Both $u(z,t)$ and $\Theta(z,t)$ rise very quickly from 0 to either the instantaneous maximum velocity or to the bulk temperature within very thin layers above the bottom plate. While after reaching its maximum value, $u(z,t)$ slowly decreases in the bulk region of the closed convection cell, $\Theta(z,t)$ reaches and stays nearly constant at the bulk temperature $\Theta = 1$. To examine the velocity and the temperature in the vicinity of plates in more detail, we plot the enlarged near-plate parts of the $u(z,t)$ and $\Theta(z,t)$ profiles in figures 2(*c*) and 2(*d*). One observes that both profiles are linear near the plate. The instantaneous velocity BL thickness $\delta_v(t)$ is then defined as the distance from the plate at which the extrapolation of the linear part of the velocity profile meets the horizontal line passing through the instantaneous maximum horizontal velocity, and the instantaneous thermal BL thickness $\delta_{th}(t)$ is obtained as the distance from the plate at which the extrapolation of the linear part of the temperature profile crosses the horizontal line passing through the bulk temperature. The arrows in figures 2(*c*) and 2(*d*) illustrate how to determine $\delta_v(t)$ and $\delta_{th}(t)$ as the crossing point distances.

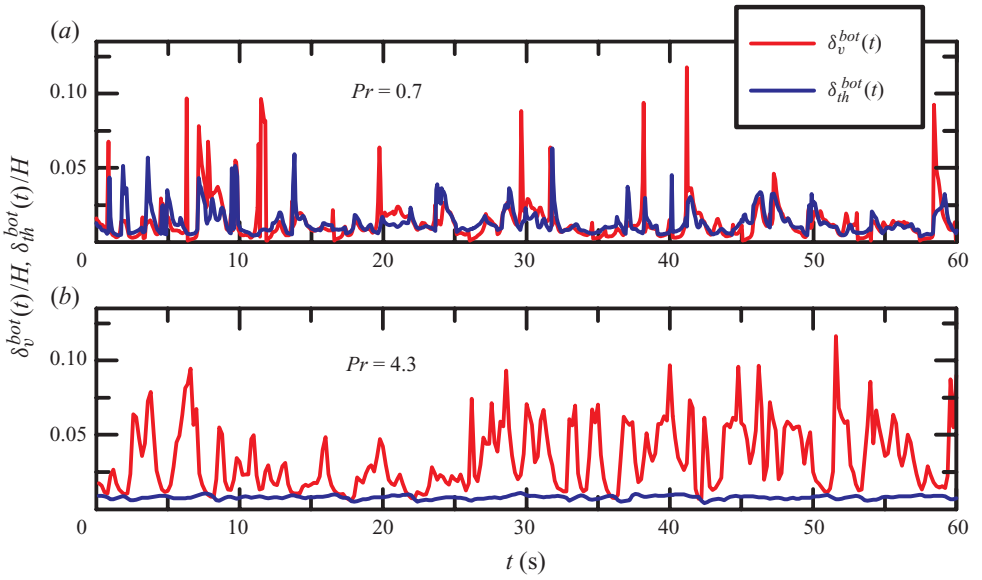

FIGURE 3. (Colour online) Sample time traces of instantaneous kinematic BL thickness, $\delta_v^{bot}(t)$ (light tinted lines) and instantaneous thermal BL thickness, $\delta_{th}^{bot}(t)$ (dark tinted lines), normalized by the cell height H. The data were obtained above the centre of the bottom plate at $Ra = 1.0 \times 10^9$ and $Pr = 0.7$ (a) and at $Ra = 1.0 \times 10^9$ and $Pr = 4.3$ (b).

Figures 3(a) and 3(b) show 60 s time traces of $\delta_v^{bot}(t)/H$ (red lines) and $\delta_{th}^{bot}(t)/H$ (blue lines) that were obtained at $Ra = 1.0 \times 10^9$ and $Pr = 0.7$ and at $Ra = 1.0 \times 10^9$ and $Pr = 4.3$, respectively. One noticeable feature is that there are two types of fluctuations: the 'normal' ones and the intermittent high peaks. For the $Pr = 0.7$ case (see figure 3a), although sometimes the peak amplitudes for the kinematic BL thickness are smaller than those for the thermal BL thickness, intermittent high peaks of $\delta_v^{bot}(t)$ and $\delta_{th}^{bot}(t)$ occur simultaneously most of time. This reflects the strong correlation between these two quantities. As we shall see in § 6, there is indeed a strong correlation between $\delta_v^{bot}(t)$ and $\delta_{th}^{bot}(t)$, and the variations of $\delta_v(t)$ lead the variations of $\delta_{th}(t)$, which suggests that these high peaks should originate from the advective passing-by of thermal plumes. For the $Pr = 4.3$ case (see figure 3b), however, the intermittent peaks for the thermal BL thickness are much less pronounced. As we shall see in § 4, due to the lack of intermittent fluctuations, the shape factor of the time-averaged thermal BL profile at $Ra = 1.0 \times 10^9$ and $Pr = 4.3$ is close to the theoretical PB value (see open triangles in figure 7b).

With measured $\delta_v(t)$ and $\delta_{th}(t)$, we can now construct the local dynamical BL frames at the plate's centre. The time-dependent re-scaled distances $z_v^*(t)$ and $z_{th}^*(t)$ from the plate in terms of $\delta_v(t)$ and $\delta_{th}(t)$, respectively, are defined as

$$z_v^*(t) \equiv \frac{z}{\delta_v(t)} \quad \text{and} \quad z_{th}^*(t) \equiv \frac{z}{\delta_{th}(t)}. \tag{3.1}$$

The dynamically time-averaged mean velocity and temperature profiles $u^*(z_v^*)$ and $\Theta^*(z_{th}^*)$, respectively, in the dynamical BL frames are then obtained by averaging over all values of $u(z,t)$ and $\Theta(z,t)$ that were measured at different discrete times t, but at the same relative positions z_v^* and z_{th}^*, respectively, i.e.

$$u^*(z_v^*) \equiv \langle u(z,t) | z = z_v^* \delta_v(t) \rangle \quad \text{and} \quad \Theta^*(z_{th}^*) \equiv \langle \Theta(z,t) | z = z_{th}^* \delta_{th}(t) \rangle. \tag{3.2}$$

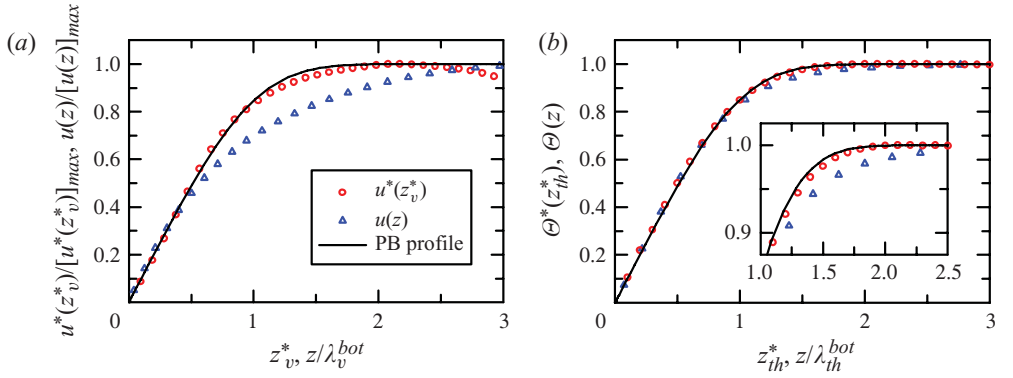

FIGURE 4. (Colour online) Comparison among (*a*) velocity profiles: dynamical frame based $u^*(z_v^*)$ (circles), laboratory frame based $u(z)$ (triangles) and the PB velocity profile (solid line); and (*b*) the corresponding temperature profiles: $\Theta^*(z_{th}^*)$ (circles), $\Theta(z)$ (triangles) and the PB temperature profile (solid line) near the bottom plate. All results obtained numerically at $Ra = 10^8$ and $Pr = 4.3$. The inset of (*b*) shows enlarged portions of the profiles around the thermal BLs' mergers with the bulk.

We first discuss our results from the simulation performed at $Pr = 4.3$, the Prandtl number corresponding to water at 40 °C. Figure 4(*a*) shows the $u^*(z_v^*)$ profile (circles), normalized by its maximum value $[u^*(z_v^*)]_{max}$, obtained at $Ra = 10^8$. For comparison, we also plot in the figure the time-averaged horizontal velocity profile $u(z)$ $(= \langle u(z,t) \rangle)$ (triangles), obtained from the same simulation. The solid line represents the PB velocity BL profile, the initial slope of which is matched to that of the measured profiles (cf. Ahlers *et al.* 2006). For the range $z_v^* \lesssim 2$, the $u^*(z_v^*)$ profile obtained in the dynamical frame agrees well with the PB profile, while the time-averaged $u(z)$ profile obtained in the laboratory frame obviously is much lower than the PB profile in the region around a few kinematic BL widths. Note that for $z_v^* \gtrsim 2$, the $u^*(z_v^*)$ profile deviates gradually from the PB profile because $u^*(z_v^*)$ decreases in the bulk region of the closed-convection system down to 0 in the centre and then changes sign. The PB profile, instead, describes the situation of an asymptotically constant, non-zero flow velocity. These DNS results are similar to those found experimentally in a rectangular cell (Zhou & Xia 2010).

Figure 4(*b*) shows a direct comparison among the temperature profiles obtained from the same simulation: the dynamical frame based $\Theta^*(z_{th}^*)$ (circles), the laboratory frame time-averaged temperature profile $\Theta(z)$ $(= \langle \Theta(z,t) \rangle)$ (triangles) and the PB temperature profile. At first glance, both $\Theta^*(z_{th}^*)$ and $\Theta(z)$ profiles are consistent with the PB thermal profile. However, looking more carefully at the region around the thermal BL to bulk merger (the inset in figure 4*b*), one notes that the $\Theta^*(z_{th}^*)$ profile obtained in the dynamical frame is significantly closer to the PB profile than the time-averaged $\Theta(z)$ profile obtained in the laboratory frame, indicating that the dynamical frame idea of Zhou & Xia (2010) works also for the thermal BL. Taken together, figures 4(*a*) and 4(*b*) illustrate that both the kinematic and the thermal BLs in turbulent RB convection are of PB type, which is a key assumption of the GL theory (Grossmann & Lohse 2000, 2001, 2002, 2004), and the dynamical frame idea of Zhou & Xia (2010) can achieve a clean separation for both temperature and velocity fields between their BL and bulk dynamics.

We now turn to the simulation performed at $Pr = 0.7$, a Prandtl number typical for gases, which is relevant in all atmospheric processes and many technical applications.

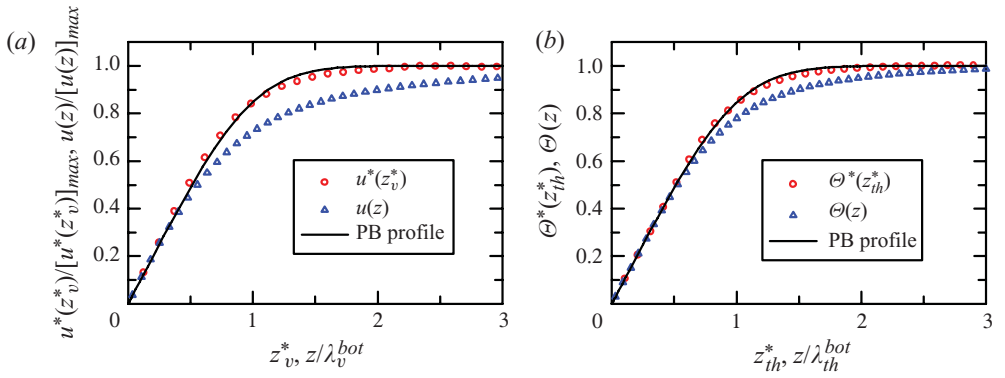

FIGURE 5. (Colour online) Comparison between (*a*) velocity profiles: dynamical $u^*(z_v^*)$ (circles), laboratory $u(z)$ (triangles) and the PB-laminar velocity profile (solid line); and (*b*) temperature profiles: dynamical $\Theta^*(z_{th}^*)$ (circles), laboratory $\Theta(z)$ (triangles) and the PB-laminar temperature profile (solid line) near the bottom plate, all obtained numerically at $Ra = 10^9$ and $Pr = 0.7$, representative for gases.

Figures 5(*a*) and 5(*b*) show direct comparisons between the temperature and velocity profiles, respectively, at $Ra = 10^9$. Again, around the BL–bulk merger range, the laboratory frame time-averaged profiles are found to be obviously lower than the PB profile. This further indicates that the time-averaged BL quantities obtained in the laboratory frame are contaminated by the mixed dynamics inside and outside the fluctuating BLs. On the other hand, within the dynamical frame, both $u^*(z_v^*)$ and $\Theta^*(z_{th}^*)$ are found to agree pretty well with the PB laminar BL profiles, indicating that the dynamical frame idea works also for the turbulent RB system with working fluids whose Prandtl numbers are of the same order as those for gases.

4. Shape factors of the velocity and temperature profiles

Let us now quantitatively compare the differences between the PB profile and the profiles obtained from both simulations and experiments for various Ra and Pr. The shapes of the velocity and temperature (thermal) profiles, labelled by $i = v$ or $i = th$, can be characterized quantitatively by their shape factors H_i, defined as (Schlichting & Gersten 2004)

$$H_i = \frac{\lambda_i^d}{\lambda_i^m}, \quad i = v, th. \tag{4.1}$$

Here λ_i^d and λ_i^m denote, respectively, the displacement and the momentum thicknesses of the profile, namely,

$$\lambda_i^d = \int_0^\infty \left[1 - \frac{Y(z)}{[Y(z)]_{max}}\right] \mathrm{d}z \quad \text{and} \quad \lambda_i^m = \int_0^\infty \left[1 - \frac{Y(z)}{[Y(z)]_{max}}\right] \frac{Y(z)}{[Y(z)]_{max}} \mathrm{d}z. \tag{4.2}$$

Here $Y(z) = u(z)$ is the velocity profile if $i = v$, and $Y(z) = \Theta(z)$ is the thermal profile if $i = th$. The deviation of these profiles from the PB profile is then measured by

$$\delta H_i = H_i - H_i^{PB}, \tag{4.3}$$

where H_i^{PB} is the shape factor for the respective PB laminar BL profile. If a given profile exactly matches the PB profile, δH_i is zero. Note that the PB velocity profile

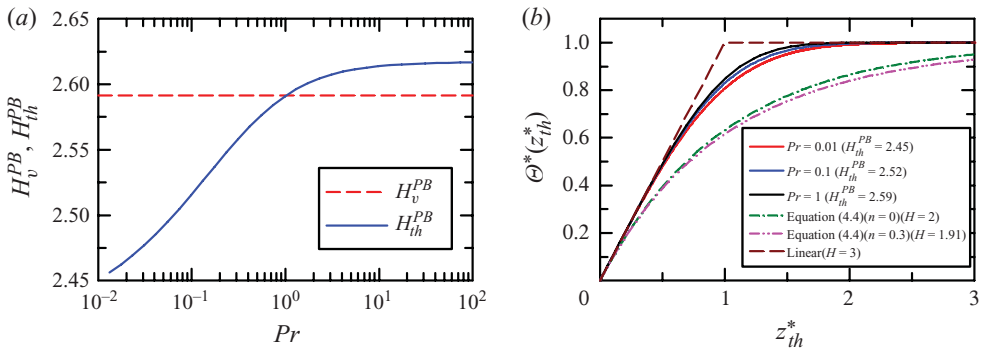

FIGURE 6. (Colour online) (*a*) The shape factors for the thermal (solid line) and velocity (dashed line) Prandtl–Blasius BL profiles as function of Pr. The asymptotic value $H_{th}^{PB}(Pr \gg 1)$ is 2.61676... and $H_v^{PB} = 2.59$. Both Prandtl–Blasius BL profiles for the velocity and for the temperature coincide for $Pr = 1$. (*b*) The thermal Prandtl–Blasius BL profiles for three Pr and the reference linear and exponential profiles, see (4.4); in the figure's resolution the thermal profile for a fourth value, $Pr = 100$, is indistinguishable from that of $Pr = 1$. Note that the shape factor of the thermal Prandtl–Blasius BL profile decreases with decreasing Pr due to the slower approach to its asymptotic level 1.

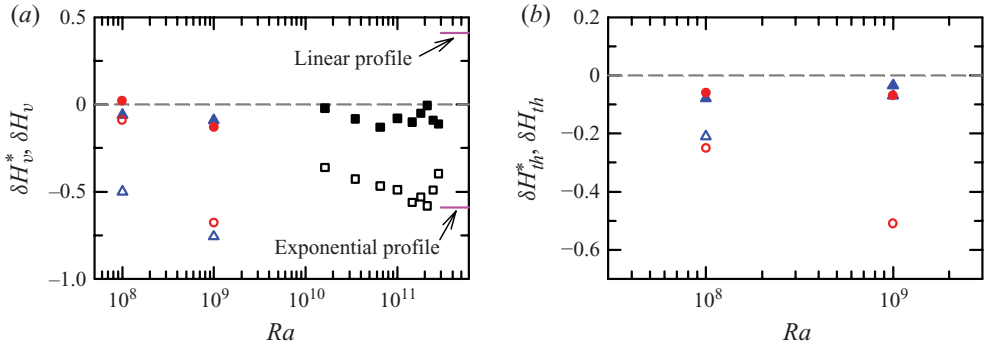

FIGURE 7. (Colour online) The Ra dependence of the deviations of the profile shape factors from the respective PB shape factors. (*a*) Laboratory frame δH_v (open symbols) and dynamical frame δH_v^* (solid symbols); (*b*) laboratory frame δH_{th} (open symbols) and dynamical frame δH_{th}^* (solid symbols); all from simulations performed at $Pr = 0.7$ (circles), $Pr = 4.3$ (triangles) and from experiments at $Pr = 5.4$ (squares).

shape factor $H_v^{PB} = 2.59$ is independent of Pr, while the thermal Prandtl–Blasius BL profile shape factor H_{th}^{PB} varies with Pr.

Figure 6(*a*) shows the shape factors $H_i(Pr)$ of the thermal and the velocity Prandtl–Blasius BL profiles as functions of Pr, and figure 6(*b*) shows the corresponding thermal profiles as functions of z_{th}^* for three different Pr. Note that the PB velocity BL profile is identical to the thermal one for $Pr = 1$. The two figures show that the thermal shape factor H_{th}^{PB} decreases with decreasing Pr. We attribute this to the decrease of the temperature profiles in the BL range and the corresponding increase of the tails for lower Pr. Thus we expect that the slower approach to the asymptotic height, 1, of the thermal profiles in the laboratory frame in figures 4 and 5 should lead to a negative deviation of their H_{th} values from the respective PB values (cf. figure 7). In contrast, a positive δH_i is obtained if the profile runs to its asymptotic level faster than the PB profile. To see this more clearly, we have also plotted two extreme cases

in figure 6(*b*), the linear and the exponential profiles. Using (4.2), one calculates the shape factor 3 for the linear profile $\Theta^*(z^*_{th}) = \min(1, z^*_{th})$ and the shape factor 2 for the exponential one $\Theta^*(z^*_{th}) = 1 - \exp(-z^*_{th})$. The H-decreasing effect by lowering the profile can also be demonstrated by analysing some profiles analytically. Using a combination of exponential profiles,

$$\Theta^*(z^*_{th}) = 0.5(1 - \exp(-(1-n)(z^*_{th})) + 0.5(1 - \exp(-(1+n)z^*_{th})), \tag{4.4}$$

with $0 \leqslant n < 1$ one can evaluate, using (4.2), that the shape factor for small n is

$$H(n) \approx H(n=0) - n^2 = 2 - n^2. \tag{4.5}$$

As shown in figure 6(*b*), the profile for $n > 0$ is below the profile for $n = 0$. This analytical example again reflects what we found as the characteristic difference between the laboratory frame profiles as compared to the dynamical frame profiles.

Figure 7(*a*) shows the velocity shape-factor deviations δH_v (open symbols) and δH^*_v (solid symbols) as obtained from simulations at $Pr = 0.7$ (circles) and $Pr = 4.3$ (triangles) as well as from experiments at $Pr = 5.4$ (squares). Here, δH_v is calculated with the time-averaged profile $u(z)$ in the laboratory frame, while δH^*_v is calculated with the dynamical, time-dependent frame profile $u^*(z^*_v)$. The laboratory frame based deviations turn out to be definitely smaller than zero. In contrast, the shape factor deviations δH^*_v for the dynamical frame profiles obviously are much closer to zero. A similar result is found for the thermal BLs: figure 7(*b*) shows δH_{th} (open symbols) and δH^*_{th} (solid symbols), versus Ra, for the same Prandtl number simulations. Again δH^*_{th} is nearly zero, whereas δH_{th} is significantly off. Thus these quantitative deviation measures indicate that the algorithm using the dynamical coordinates can effectively disentangle the mixed dynamics inside and outside the fluctuating BLs.

5. The shape of instantaneous velocity and temperature profiles

To further understand the results of our dynamical re-scaling method, we study the instantaneous velocity and temperature profiles. Figures 8, 9 and 10 show examples of instantaneous velocity and temperature profiles, where the distance from the plate, z, has been normalized by the instantaneous BL thickness corresponding to that moment and the velocity has been normalized by the instantaneous maximum horizontal velocity. In these figures, we also plot the PB profiles for comparison and give the instantaneous shape factors. It is seen that most of the time both the velocity and temperature BL profiles are of PB type; instantaneous deviations are associated with plume detachments. We note that averaging all these 're-scaled' profiles corresponds to the averaging of (3.2). On the other hand, a simple average of the 'unscaled' profiles will distort the shape of the profiles from that of Prandtl–Blasius because of the mixing between BL and bulk dynamics, owing to the fluctuations of the BL thickness. This also explains why our method works, i.e. averages of the normalized instantaneous profiles will naturally separate the BL and bulk dynamics, as they are all expressed in the intrinsic BL-length scale, which in this case is time-dependent. The properties of the instantaneous profiles can be quantified by their time-dependent shape factor $H_i(t)$ ($i = v$ or th). Again, we examine the shape-factor difference $\delta H_i(t) = H_i(t) - H_i^{PB}$ for the respective instantaneous profiles and that of the PB profile H_i^{PB}. Figures 11(*a*) and 11(*b*) show the probability density functions (PDFs) of $\delta H_i(t)$ for the experimental and numerical velocity profiles, respectively. Overall, these PDFs are all peaked close zero, showing that most of the time the velocity profiles are indeed of PB type. For the experimental results, the distributions

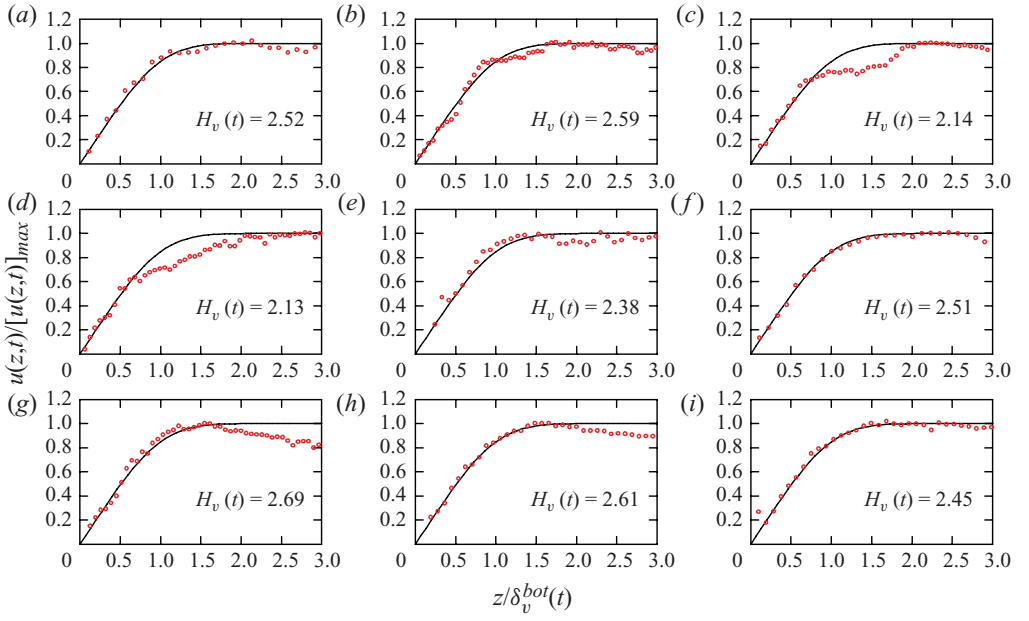

FIGURE 8. (Colour online) Examples of experimental instantaneous horizontal velocity profiles measured at $Ra = 1.8 \times 10^{11}$ and $Pr = 5.4$, and re-scaled by the instantaneous kinematic BL thickness and maximum velocity. Here the time average $[u(z)]_{max}$ is 2.2 cm s^{-1}, and δ_v has a most probable value of $0.004\,H$. We also give the instantaneous shape factors. The solid curves are the PB velocity profiles. These examples (and those in figures 8 and 9) are chosen to show various shapes of profiles observed: the majority have excellent agreement with the PB profile.

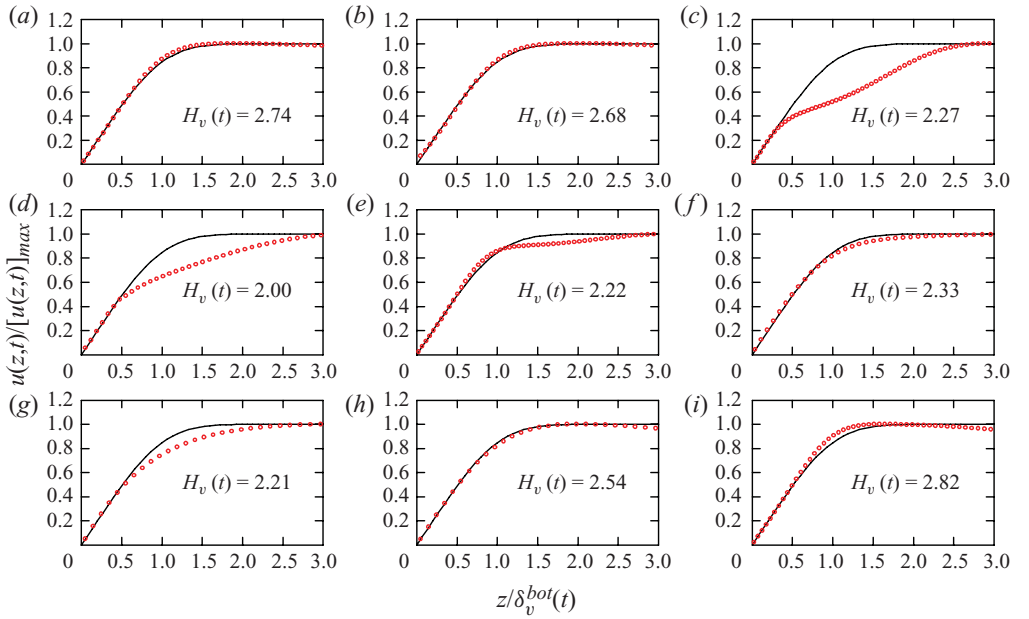

FIGURE 9. (Colour online) Examples of re-scaled instantaneous horizontal velocity profiles obtained numerically at $Ra = 10^9$ and $Pr = 0.7$. The mean $[u(z)]_{max}$ is 8.0 cm s^{-1} (corresponding to a Reynolds number of $[u(z)]_{max} H/\nu \approx 19\,100$) and δ_v has a most probable value of $0.01\,H$. The solid curves are the PB velocity profiles.

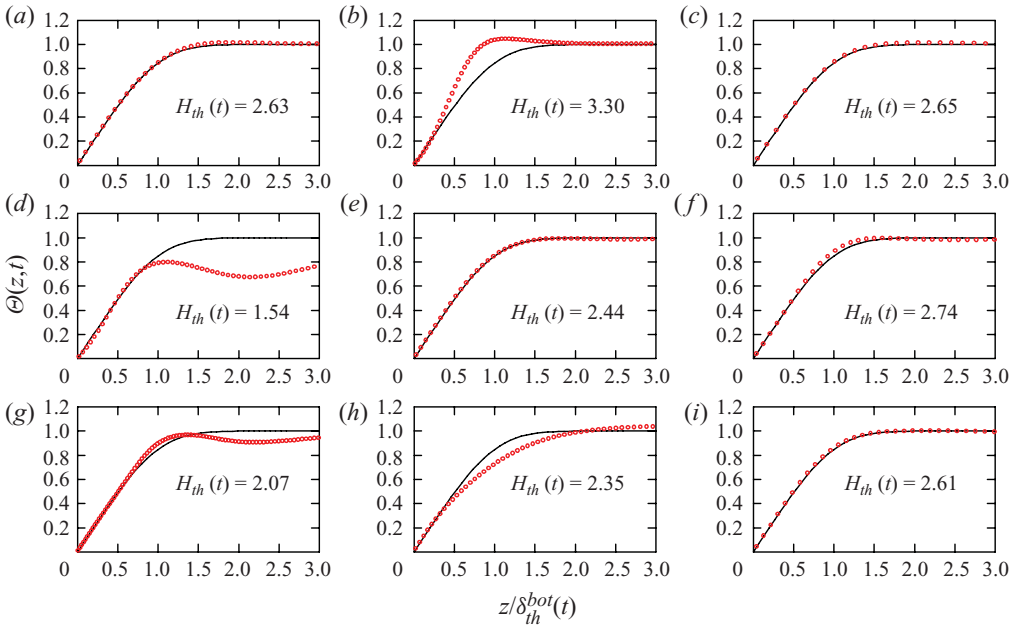

FIGURE 10. (Colour online) Examples of re-scaled instantaneous temperature profiles obtained numerically at $Ra = 10^9$ and $Pr = 0.7$. The solid curves are the PB temperature profiles. Here δ_{th} fluctuates about its most probable value of $0.012\,H$.

are exactly peaked at zero, except that for the highest $Ra = 2.5 \times 10^{11}$, for which the maximum is slightly off. In addition, comparing to DNS data, the experimental data have broader distributions, which is presumably due to their larger values of Ra (hence greater fluctuations). This is consistent with our analysis in § 4 that a more turbulent profile should approach its asymptotic value slower than the PB profile and thus give rise to a negative value of δH_v. The peaks for the numerical data are a bit off zero. These data may also suggest that the PDFs of the shape factors are slightly dependent on Pr. Note that there is a minor peak located at $\delta H_v(t) \simeq -0.8$ for the data set $Ra = 10^9$ and $Pr = 0.7$. While we do not know why only this set exhibits this behaviour, it is interesting to note that the instantaneous profile shown in figure 2(*c*) has a shape factor $H_v = 1.8$ which corresponds to exactly the shape factor of the minor peak here.

In figure 11(*c*), we show the PDFs for $\delta H_{th}(t)$ from the DNS temperature data. In the examined regime, these PDFs are independent of Pr, but show a certain Ra-dependence. While the high Ra data are peaked exactly at zero, the low Ra data show a minor peak or hump at a negative value. This suggests that there are temperature profiles that have a much slower approach to the asymptotic value. For example see the plot in figure 10(*d*): here one can observe that at the position around the BL thickness, $\Theta \simeq 0.8$, i.e. the temperature at the edge of the BL only reaches about 80 % of the asymptotic value. This distortion of the BL profile is probably caused by a plume emission that thins the BL thickness corresponding to that instant, while the temperature adjacent to the BL is not able to instantly relax back to the bulk value. Recall that the instantaneous thermal BL thickness is defined through the asymptotic value of Θ (see figure 2*d*). If we, however, define the BL thickness as the intersection between the extrapolations of the linear part of the profile and its 'first maximum', the

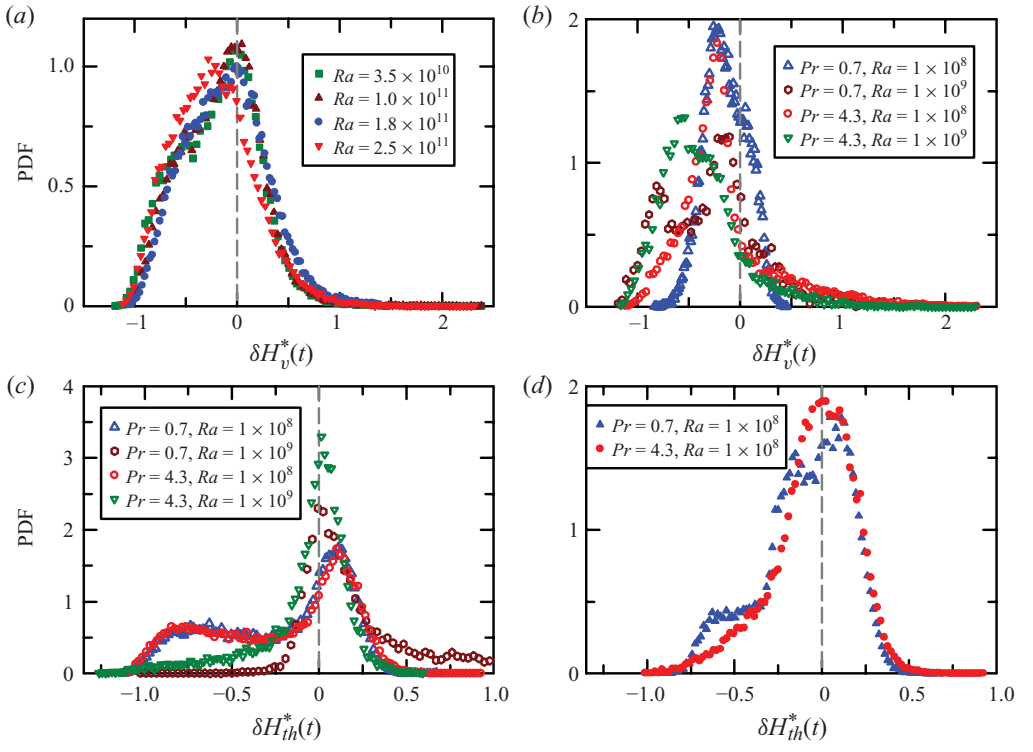

FIGURE 11. (Colour online) PDFs of the shape-factor difference between those of the re-scaled instantaneous profiles and those of the corresponding PB profiles. (*a*) Experimental velocity data, (*b*) DNS velocity data, (*c*) DNS temperature data (profiles saturate at bulk temperature) and (*d*) DNS temperature data (profiles saturate at first maximum). See text for explanation.

re-scaled instantaneous profile looks quite different. Indeed, following this procedure, we can obtain temperature profiles that are much closer to the PB type. Figure 11(*d*) shows the PDFs of the shape factor difference for instantaneous re-scaled temperature profiles obtained this way. The figure shows that the PDFs for the data sets $Ra = 10^8$, $Pr = 0.7$ and 4.3 now peak at zero and the minor peak seen in figure 11(*c*) is either gone or significantly reduced. We stress, however, that here we use the first maximum instead of the asymptotic value of the temperature profile in the determination of the thermal BL thickness only for the purpose of gaining a better understanding. In order to have a consistent and uniform procedure, all the BL thicknesses presented in this paper are obtained using the more 'traditional' definitions, i.e. those shown in figure 2.

6. Relationship between $\delta_v(t)$ and $\delta_{th}(t)$

The relation between $\delta_v(t)$ and the external large-scale velocity field has been discussed in detail in Zhou & Xia (2010). Here, we further study the relation between the measured instantaneous kinematic and thermal BL thicknesses. We calculate the cross-correlation function between $\delta_v(t)$ and $\delta_{th}(t)$, i.e. $g(\tau) = \langle [\delta_v(t) - \langle \delta_v(t) \rangle][\delta_{th}(t+\tau) - \langle \delta_{th}(t) \rangle] \rangle / \sigma_v \sigma_{th}$, where $\sigma_v = \sqrt{\langle [\delta_v(t) - \langle \delta_v(t) \rangle]^2 \rangle}$ and $\sigma_{th} = \sqrt{\langle [\delta_{th}(t) - \langle \delta_{th}(t) \rangle]^2 \rangle}$. Figure 12 shows two examples of $g(\tau)$ measured at $Pr = 4.3$ and 0.7, respectively. Two noteworthy features are as follows: (i) there is a strong positive correlation between

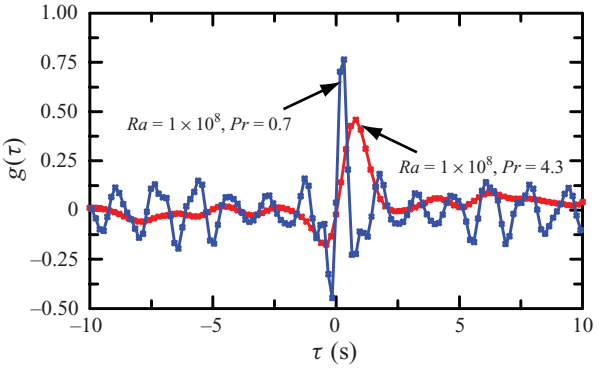

FIGURE 12. (Colour online) Cross-correlation function $g(\tau)$ between $\delta_v(t)$ and $\delta_{th}(t)$.

$\delta_v(t)$ and $\delta_{th}(t)$, i.e. a thicker kinematic BL leads to a thicker thermal BL and vice versa; (ii) the positive peak is located at a positive time lag τ_0, indicating that the variations of $\delta_v(t)$ lead the variations of $\delta_{th}(t)$. One can also see that τ_0 for $Pr = 4.3$ is larger than τ_0 for $Pr = 0.7$. The reason for this behaviour is that the kinematic BL is thicker than the thermal one at $Pr = 4.3$, and hence, a longer time lag is needed for the influence of the kinematic BL to propagate to the thermal BL via momentum diffusion, while the two layers are of the same order at $Pr = 0.7$. This result provides direct evidence for the interplay between the kinematic BL and the thermal BL.

We also notice oscillations in the cross-correlation functions, which are rather robust for the lower Pr data. The time scale of this oscillation is of the order of 1.5 s (3 s) for $Pr = 0.7$ ($Pr = 4.3$). This is comparable to $H/[u(z)]_{max}$, which equals 1.58 s (3.02 s). This immediately suggests a connection to the periodic plume emission model of Villermaux (1995). However, from watching movies of the respective flows, we conclude that the flow organization is more complicated than suggested in that model: next to the large-scale convection roll, corner-flow develops (see Sugiyama *et al.* 2010). Plumes emitted from the BL are first collected by the corner flow and then partly emitted again. These plumes then hit the thermal BL from the top, leading to further plume emission. This periodic process is more pronounced and more stable at $Pr = 0.7$, leading to stronger long-time correlations. On the other hand, in a 3D system, Xi *et al.* (2009) and Zhou *et al.* (2009) have shown experimentally that thermal plumes are emitted neither periodically nor alternately, but randomly and continuously, from the top and bottom plates. We note that Villermaux's model is 2D and the present numerical simulation is also 2D. Then oscillations observed here might be a major difference between the 2D and 3D systems. Further study beyond the scope of this paper will be required to fully settle this issue.

7. Conclusions

In summary, we have studied the velocity and temperature BL profiles in turbulent RB convection both numerically and experimentally. We extended previous results to different Prandtl numbers and, in particular, to thermal BLs. The results show that both the velocity and the temperature BLs (at least in the plates' centre region) are of laminar PB type in the co-moving dynamical frame in turbulent thermal convection for the parameter ranges studied. However, the fluctuations of the BL widths, induced by the fluctuations of the large-scale mean flow and the emissions of thermal plumes, cause measuring probes at fixed heights above the plate to sample a mixed dynamics,

one pertaining to the BL range and the other one pertaining to the bulk. This is the reason why the time-averaged velocity and temperature profiles measured in previous studies in fixed laboratory (RB cell) frames deviate from the PB profiles. To disentangle that mixed dynamics, we constructed a dynamical BL frame that fluctuates with the instantaneous BL thicknesses. Within this dynamical frame, both velocity and temperature profiles are very consistent with the classical PB laminar BL profiles, both for lower and larger *Pr* (from 0.7 to 5.4). Furthermore, when the instantaneous velocity and temperature are re-scaled by their respective instantaneous BL thicknesses, we find that the PB profiles not only hold in a time-averaged sense, but most of the time also in an instantaneous sense. We have thus extended the time-independent Blasius BL equation or the Prandtl–Blasius BL to the time-dependent case, in the sense that it holds at every instant in the frame that fluctuates with the instantaneous BL thickness.

To conclude, we have validated the idea and algorithm of using dynamical coordinates over a range of *Pr* and *Ra* for both kinematic and thermal BLs and have shown that the PB laminar BL profile is a valid description for the BLs of both velocity and temperature in turbulent thermal convection. Laminar Prandtl–Blasius BL theory in turbulent RB thermal convection has thus turned out to indeed be valid not only in terms of the scaling properties, but also in terms of BL profiles as seen from the dynamical frame, co-moving with the local, instantaneous BL widths.

We thank E. S. C Ching for helpful discussions. We gratefully acknowledge support of this study by the Natural Science Foundation of Shanghai (No. 09ZR1411200), 'Chen Guang' project (No. 09CG41), and 'Pu Jiang' project (No. 10PJ1404000)(Q.Z.), by the Research Grants Council of Hong Kong SAR (Nos. CUHK403806 and 403807) (K.Q.X.) and by the research programme of FOM, which is financially supported by NWO (R.J.A.M.S. and D.L.).

REFERENCES

Ahlers, G., Brown, E., Fontenele Araujo, F., Funfschilling, D., Grossmann, S. & Lohse, D. 2006 Non-Oberbeck–Boussinesq effects in strongly turbulent Rayleigh–Bénard convection. *J. Fluid Mech.* **569**, 409–445.

Ahlers, G., Calzavarini, E., Fontenele Araujo, F., Funfschilling, D., Grossmann, S., Lohse, D. & Sugiyama, K. 2008 Non-Oberbeck–Boussinesq effects in turbulent thermal convection in ethane close to the critical point. *Phys. Rev.* E **77**, 046302.

Ahlers, G., Fontenele Araujo, F., Funfschilling, D., Grossmann, S. & Lohse, D. 2007 Non-Oberbeck–Boussinesq effects in gaseous Rayleigh–Bénard convection. *Phys. Rev. Lett.* **98**, 054501.

Ahlers, G., Grossmann, S. & Lohse, D. 2009 Heat transfer and large scale dynamics in turbulent Rayleigh–Bénard convection. *Rev. Mod. Phys.* **81**, 503–537.

Castaing, B., Gunaratne, G., Heslot, F., Kadanoff, L., Libchaber, A., Thomae, S., Wu, X.-Z., Zaleski, S. & Zanetti, G. 1989 Scaling of hard thermal turbulence in Rayleigh–Bénard convection. *J. Fluid Mech.* **204**, 1–30.

Ching, E. S. C. 1997 Heat flux and shear rate in turbulent convection. *Phys. Rev.* E **55**, 1189–1192.

Dubrulle, B. 2001 Logarithmic corrections to scaling in turbulent thermal convection. *Eur. Phys. J.* B **21**, 295–304.

Dubrulle, B. 2002 Scaling in large Prandtl number turbulent thermal convection. *Eur. Phys. J.* B **28**, 361–367.

Grossmann, S. & Lohse, D. 2000 Scaling in thermal convection: a unifying theory. *J. Fluid Mech.* **407**, 27–56.

Grossmann, S. & Lohse, D. 2001 Thermal convection for large Prandtl numbers. *Phys. Rev. Lett.* **86**, 3316–3319.

Grossmann, S. & Lohse, D. 2002 Prandtl and Rayleigh number dependence of the Reynolds number in turbulent thermal convection. *Phys. Rev.* E **66**, 016305.

Grossmann, S. & Lohse, D. 2004 Fluctuations in turbulent Rayleigh–Bénard convection: the role of plumes. *Phys. Fluids* **16**, 4462–4472.

Lohse, D. & Xia, K.-Q. 2010 Small-scale properties of turbulent Rayleigh–Bénard convection. *Annu. Rev. Fluid Mech.* **42**, 335–364.

Malkus, M. V. R. 1954 The heat transport and spectrum of thermal turbulence. *Proc. R. Soc. Lond.* A **225**, 196–212.

du Puits, R., Resagk, C. & Thess, A. 2007 Mean velocity profile in confined turbulent convection. *Phys. Rev. Lett.* **99**, 234504.

Qiu, X.-L. & Xia, K.-Q. 1998 Viscous boundary layers at the sidewall of a convection cell. *Phys. Rev.* E **58**, 486–491.

Schlichting, H. & Gersten, K. 2004 *Boundary Layer Theory*, 8th edn. Springer.

Shishkina, O. & Thess, A. 2009 Mean temperature profiles in turbulent Rayleigh–Bénard convection of water. *J. Fluid Mech.* **633**, 449–460.

Shraiman, B. I. & Siggia, E. D. 1990 Heat transport in high-Rayleigh-number convection. *Phys. Rev.* A **42**, 3650–3653.

Siggia, E. D. 1994 High-Rayleigh-number convection. *Annu. Rev. Fluid Mech.* **26**, 137–168.

Stevens, R. J. A. M., Verzicco, R. & Lohse, D. 2010 Radial boundary layer structure and Nusselt number in Rayleigh–Bénard convection. *J. Fluid Mech.* **643**, 493–507.

Sugiyama, K., Calzavarini, E., Grossmann, S. & Lohse, D. 2009 Flow organization in non-Oberbeck–Boussinesq Rayleigh–Bénard convection in water. *J. Fluid Mech.* **637**, 105–135.

Sugiyama, K., Ni, R., Stevens, R. J. A. M., Chan, T.-S., Zhou, S.-Q., Xi, H.-D., Sun, C., Grossmann, S., Xia, K.-Q. & Lohse, D. 2010 Flow reversals in thermally driven turbulence. *Phys. Rev. Lett.* **105**, 034503.

Sun, C., Cheung, Y.-H. & Xia, K.-Q. 2008 Experimental studies of the viscous boundary layer properties in turbulent Rayleigh–Bénard convection. *J. Fluid Mech.* **605**, 79–113.

Villermaux, E. 1995 Memory-induced low frequency oscillations in closed convection boxes. *Phys. Rev. Lett.* **75**, 4618–4621.

Xi, H.-D., Zhou, S.-Q., Zhou, Q., Chan, T.-S. & Xia, K.-Q. 2009 Origin of the temperature oscillation in turbulent thermal convection. *Phys. Rev. Lett.* **102**, 044503.

Xia, K.-Q., Sun, C. & Zhou, S.-Q. 2003 Particle image velocimetry measurements of the velocity field in turbulent thermal convection. *Phys. Rev.* E **68**, 066303.

Zhou, Q., Xi, H.-D., Zhou, S.-Q., Sun, C. & Xia, K.-Q. 2009 Oscillations of the large-scale circulation in turbulent Rayleigh–Bénard convection: the sloshing mode and its relationship with the torsional mode. *J. Fluid Mech.* **630**, 367–390.

Zhou, Q. & Xia, K.-Q. 2010 Measured instantaneous viscous boundary layer in turbulent Rayleigh–Bénard convection. *Phys. Rev. Lett.* **104**, 104301.